

Potential Induced Changes in Neuromedin B Adsorption on Ag, Au, and Cu Electrodes Monitored by Surface-Enhanced Raman Scattering

Ilja Ignatjev,[†] Edyta Podstawka-Proniewicz,^{*,‡} Gediminas Niaura,^{*,†} John R. Lombardi,[§] and Leonard M. Proniewicz[‡]

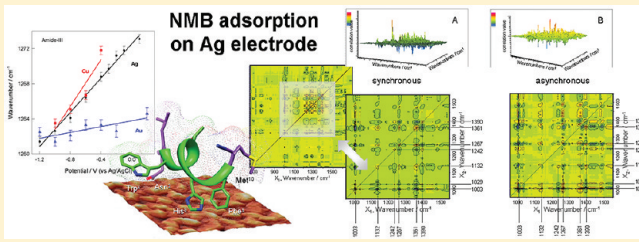
[†]Institute of Chemistry, Center for Physical Sciences and Technology, A. Gostauto 9, LT-01108, Vilnius, Lithuania

[‡]Faculty of Chemistry, Jagiellonian University, ul. Ingardena 3, 30-060 Krakow, Poland

[§]Department of Chemistry, City College of New York, 160 Convent Avenue, New York, New York 10031, United States

Supporting Information

ABSTRACT: Surface-enhanced Raman scattering (SERS), electrochemistry, and generalized two-dimensional correlation analysis (G2DCA) methods were used to define neuromedin B (NMB) ordered superstructures on Ag, Au, and Cu electrode surfaces at different applied electrode potentials in an aqueous solution at physiological pH. The orientation of NMB and the adsorption mechanism were determined based on the analysis of enhancement, broadness, and shift in wavenumber of particular bands, which allow drawing some conclusions about NMB geometry and changes in this geometry upon change of the electrode type and applied electrode potential. The presented data demonstrated that NMB deposited onto the Ag, Au, and Cu electrode surfaces showed bands due to vibrations of the moieties that were in contact/close proximity to the electrode surfaces and thus were located on the same side of the polypeptide backbone. These included the Phe⁹ and Trp⁴ rings, the sulfur atom of Met¹⁰, and the –CCN– and –C=O units of Asn². However, some subtle variations in the arrangement of these fragments upon changes in the applied electrode potential were distinguished. The Amide-III vibrations exhibited an electrochemical Stark effect (potential dependent frequencies) with Stark tuning slope sensitive to the electrode material. Potential-difference spectrum revealed that the imidazole ring of His⁸ was bonded to the Cu electrode surface at relatively positive potentials.



INTRODUCTION

The understanding of the bonding of peptides to a metal surface is critically important for a number of fundamental and applied fields including biocatalysis, bioelectrochemistry, construction of biosensors, and biomaterials biocompatibility analysis.^{1–4} Neuromedin B (NMB, (H-Gly-Asn-Leu-Trp-Ala-Thr-Gly-His-Phe-Met-NH₂)) (see Figure 1) is a bombesin-related peptide in mammals originally isolated from the pig spinal cord.⁵ Subsequently, it was detected in the human central nervous system (CNS) and gastrointestinal tract.⁶ This small peptide plays important functions in CNS and peripheral tissues, including regulation of exocrine and endocrine secretions, cell growth, body temperature, blood pressure, and glucose level.⁷ Recently, it was found to be involved in the progression of cancer diseases.⁸ However, the mechanism of this action still remains unknown. Therefore, it is important to evaluate the contribution of each of the NMB structural components in affecting its distinct physiological response to a G protein-coupled seven-transmembrane NMB-preferring subtype receptor (rNMB-R). Structural analysis of such peptide and its recognition on a picomolar basis (10–100 pM) require a technique that must be molecule specific and highly sensitive. Surface-enhanced Raman spectroscopy (SERS) fulfills these criteria, allowing elucidation of molecular

structure of adsorbed species and surface processes at the submonolayer level.^{9–13} Previously, we have utilized the SERS technique to probe adsorption states of bombesin, neuromedin C (NMC), and other bombesin-related peptides and fragments in Ag sol^{14–17} and on Ag, Au, and Cu electrodes.^{18–23} Recently, for frog, pig, and human neurotensin (NT), human single-site mutants, and specifically modified neurotensin fragments, we have correlated the contribution of the structural components to their ability to interact with a neurotensin subtype 1 G protein-coupled superfamily receptor (NTR1) using SERS pattern.^{24,25} This has been done on the strength of the comparison of the information gathered from the biological studies that have shown which amino acids from the peptide backbone were involved in the peptide–receptor interaction with the information received from SERS studies that have shown which amino acids from the peptide backbone interacted with a metal surface. On the other hand, those which are suggested not to have direct influence on the substrate-receptor binding are also not active in SERS, i.e., their modes are not seen in the SERS spectra. In these cases, the

Received: March 22, 2011

Revised: August 3, 2011

Published: August 03, 2011

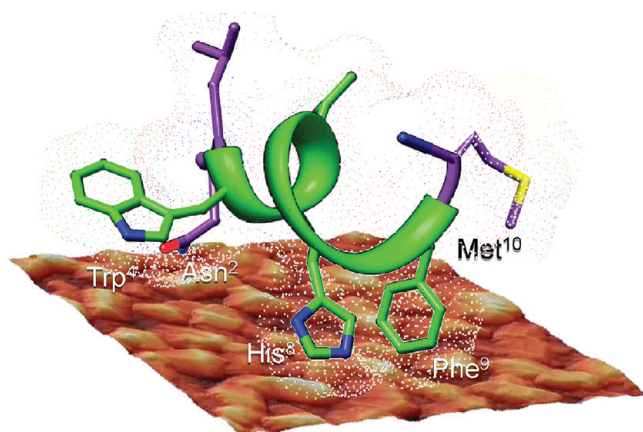


Figure 1. NMR solution structure of NMB in a membrane-mimetic environment (RSCB Protein Data Bank, Id 1C9A.pdb, ref 33). Possible mechanism of NT interaction with a metal electrode surface.

same amino acids (peptide fragments) have participated in the interaction with the receptor as well as electrochemically roughened Ag substrate. These studies have demonstrated the importance of the nature of the electrode and amino acid sequence of the investigated peptide on its adsorption properties and the architecture of the surface-bound peptide–metal complex. Potential-dependent measurements combined with generalized two dimensional correlation analysis (G2DCA) provide an additional parameter for determination of magnitude, direction, and sequence of the observed, even slight, alternations in the peptide adsorbed state upon changes of the electrode charge.^{18–20} In addition, the use of an aqueous solution afforded by Raman spectroscopy provides an opportunity toward understanding the peptide surface phenomena at physiological conditions. Within this context, we used SERS, electrochemistry, and G2DCA methods to define NMB ordered superstructures on the Ag, Au, and Cu electrode surfaces at different applied electrode potentials in the aqueous solution.

■ EXPERIMENTAL SECTION

Chemicals. Salts, inorganic acids, and alkalies of ACS reagent grade were purchased from Sigma-Aldrich GmbH (Germany). The Millipore purified water ($18 \text{ M}\Omega \text{ cm}$) was used. NMB was purchased from Bachem Co. (Switzerland). Its purity and chemical structure were verified by taking ^1H and ^{13}C NMR spectra using a Bruker Avance DRX 300 MHz spectrometer and by mass spectrometry performed with a Finnigan Mat TSQ 700 instrument.

SERS Measurements. The spectroelectrochemical instrumentation has been described in detail elsewhere.¹⁸ SERS spectra were recorded using an Echelle spectrometer RamanFlex 400 (PerkinElmer, Inc.) equipped with a thermoelectrically cooled (-50°C) charge-coupled device (CCD) detector and fiber optic cable for excitation and collection of the spectra. Excitation was provided by a 785 nm diode laser. The excitation/collection geometry was 180° . The laser power at the sample was set at 50 mW, and the laser beam was focused on a $200 \mu\text{m}$ diameter spot on the metal surface. Spectral acquisition times were 300 s. The wavenumber axis was calibrated using the polystyrene standard (ASTM E 1840), yielding a $\pm 1 \text{ cm}^{-1}$ absolute wavenumber accuracy for sharp bands. Intensities were calibrated by

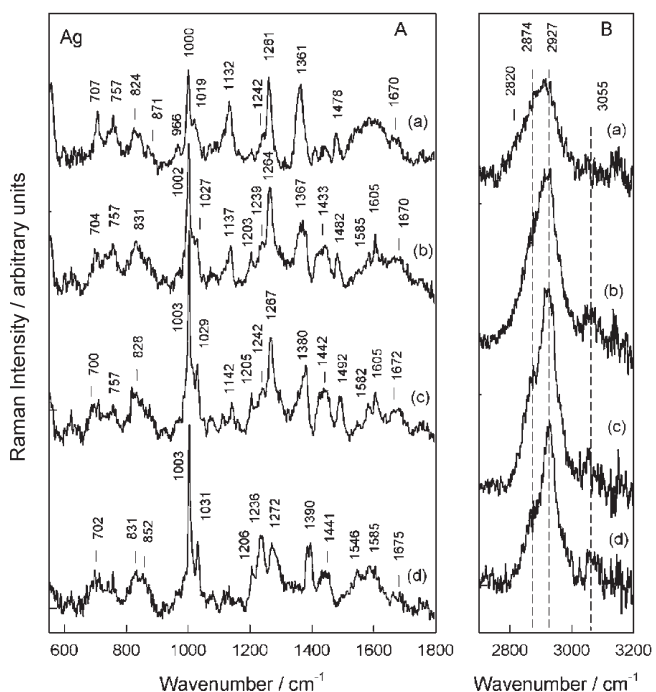


Figure 2. SERS spectra of NMB adsorbed on a roughened Ag electrode at -1.200 V (a), -0.800 V (b), -0.400 V (c), and 0.100 V (d) electrode potentials. Measurement conditions: $0.1 \text{ M Na}_2\text{SO}_4$ solution containing 0.01 M phosphate buffer (pH 7.0) and 10^{-5} M of NMB; excitation wavelength, 785 nm ; laser power at the sample, 50 mW ; integration time, 300 s .

the NIST intensity standard (SRM 2241). Spectroelectrochemical measurements were carried out in a cylinder-shaped three electrode cell with a quartz circular window, arranged with a flat circular working electrode (Ag, Au, or Cu) of ca. 5 mm in diameter, press-fitted into the Teflon rod. The working electrode was placed at approximately 3 mm distance from the cell window. Pt wire and KCl-saturated Ag/AgCl electrodes were used as counter and reference electrodes, respectively. Potential values reported below refer to this reference electrode. To remove the laser beam-induced photo- and thermo-effects, the cell together with the electrodes were moved linearly with respect to the laser beam with a rate of $15–25 \text{ mm/s}$ using custom built equipment.^{26,27} To eliminate oxygen during the experiments, solution was continuously bubbled with ultra pure Ar gas.

Electrode Preparation for SERS. Before measurements, the Ag, Au, and Cu electrodes were polished with soft sandpaper (P2500) and a $0.05 \mu\text{m}$ alumina slurry (Stuers, Denmark) for refreshing the surface. Then, the electrodes were sonicated in water–ethanol mixture (1:1) for 10 min.

Before roughening, the Au electrode was cleaned electrochemically in a $0.5 \text{ M H}_2\text{SO}_4$ aqueous solution by the following two-step procedure. First, the electrode was subjected to $3–5$ oxidation–reduction cycles in the potential range between 2.100 and 0.000 V with a 100 mV/s scan rate. After that, 20 oxidation–reduction cycles were made in the potential range of $0.000–1.600 \text{ V}$. Then, the electrode was rinsed with ultrapure water and transferred into the electrode roughening cell filled with 0.1 M NaCl solution, and the potential was first kept at -1.0 V for 1 min.

Electrochemical roughening procedure of the Au electrode was performed by the 50-fold potential scanning from -0.300 to

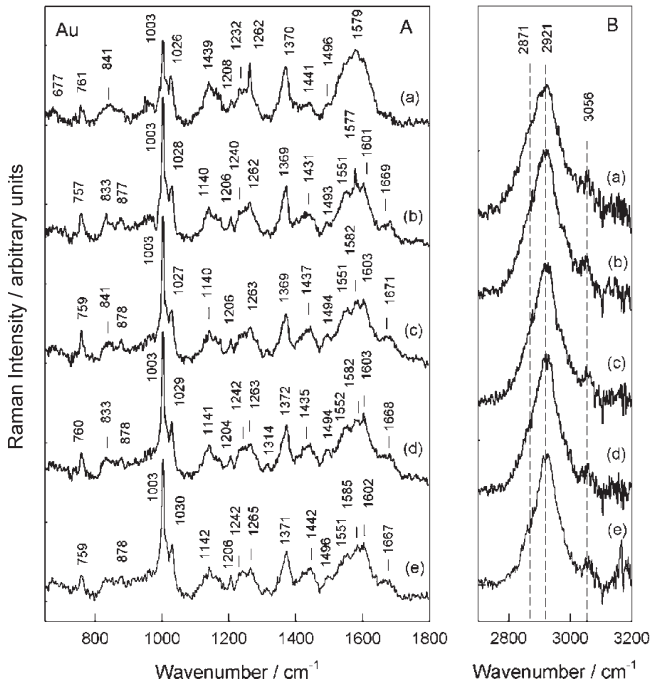


Figure 3. SERS spectra of NMB adsorbed on a roughened Au electrode at -1.200 V (a), -0.800 V (b), -0.400 V (c), -0.200 V (d), and 0.200 V (e) electrode potentials. Measurement conditions: 0.1 M Na_2SO_4 solution containing 0.01 M phosphate buffer (pH 7.0) and 10^{-5} M of NMB; excitation wavelength, 785 nm; laser power at the sample, 50 mW; integration time, 300 s.

1.300 V (scan rate 500 mV/s) with pause for 90 s at the negative and 2 s at the positive potentials,^{28,29} while the Ag electrode was roughened in 0.1 M NaCl solution using five oxidation-reduction cycles in the potential range between -0.600 and 0.600 V (scan rate 1200 mV/s) with pause for 30 s at the negative and 10 s at the positive potentials.³⁰ The Cu electrode after polishing was transferred into the cell containing 0.02 M CuSO₄ with pH adjusted to 4.5 and SERS active fresh Cu layer was electrodeposited at $E = -0.50$ V for 3 min.³¹ The cleanliness of the electrodes was checked by SERS before introduction of NMB (Figure S1, Supporting Information).

Generalized Two-Dimensional Correlation Analysis. G2DCA of the SERS spectra of NMB adsorbed on the Ag, Au, and Cu electrodes was performed using SpectraCorr version 1.1 SP1 software, by Thermo Fisher Scientific Inc., 2004–2007. The four/five potential-dependent SERS spectra of NMB were normalized and used to generate G2D maps.

Spectral Analysis. Spectral analysis presented in this work was performed using GRAMS/AI 8.0 (Thermo Electron Corp.) software.

■ RESULTS AND DISCUSSION

Figures 2–4 compare the SERS spectra of NMB adsorbed on the Ag, Au, and Cu electrode surfaces, respectively, at physiological pH in the electrode potential range from -1.200 to 0.200 V. The position of the enhanced bands in these spectra, given in inverse centimeters, are gathered in Table 1 along with both the appropriate vibrational assignments and the frequencies of the bands observed in the ordinary Raman spectrum of the solid species. Because the NMB Raman spectra previously published have been well-defined,²³ it is not shown and discussed here.

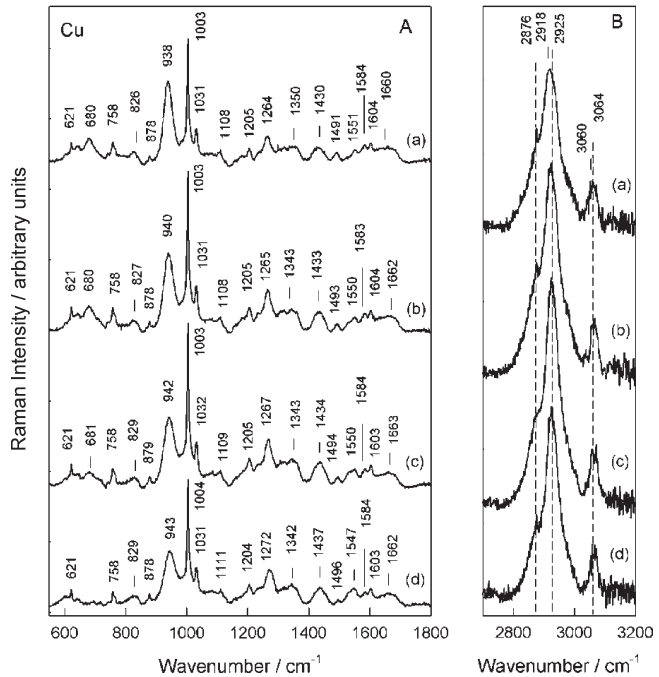


Figure 4. SERS spectra of NMB adsorbed on a roughened Cu electrode at -1.000 V (a), -0.800 V (b), -0.600 V (c), and -0.400 V (d) electrode potentials. Measurement conditions: 0.1 M Na_2SO_4 solution containing 0.01 M phosphate buffer (pH 7.0) and 10^{-5} M of NMB; excitation wavelength, 785 nm; laser power at the sample, 50 mW; integration time, 300 s.

Likewise, the SERS spectra of NMB in a Ag sol and onto electrochemically roughened Ag substrate have already been analyzed in detail,^{15,23} thus we have not refined the band assignments here. In this work we examined the enhancement, broadness, and shift in wavenumber of particular bands, which allowed drawing some conclusions about the geometry of the adsorbed NMB and the changes in this geometry upon change of the electrode type and applied electrode potential. As expected, these spectra almost exclusively possess the SERS bands characteristic of vibrations of L-phenylalanine at the 9 position (Phe⁹) and L-tryptophane at the 4 position of the NMB amino acid sequence (Trp⁴). In addition, spectral features from the –CCN– and –C=O units of L-asparagine at the 2 position (Asn²), the S–C– bond of L-methionine at the 10 position (Met¹⁰), the peptide bond, and the methyl/methylene moiety were observed. Potential–difference spectra also revealed that the imidazole ring of His⁸ was bonded to the Cu electrode surface at the relatively positive potentials. However, a broad and intense band near 940–960 cm⁻¹ resulted from the phosphate anions adsorbed at the Cu electrode surface.³² Therefore, the SERS spectra presented here demonstrate that NMB deposited onto the Ag, Au, and Cu electrode surfaces show bands due to vibrations of the moieties that were in contact/close proximity to the electrode surfaces and thus should be located on the same side of the polypeptide backbone. These include the Phe⁹ and Trp⁴ rings, the sulfur atom of Met¹⁰, the –CCN– and –C=O units of Asn², and His⁸. As is evident from the solution structure of NMB in the membrane-mimetic environments (Figure 1),³³ the aforementioned positions in the sequence fit these requirements. A detailed analysis of the spectral changes induced by the applied electrode potential observed for the aforementioned moieties

Table 1. Wavenumbers and Proposed Band Assignments for the Raman and SERS Spectra of NMB in Solid State and Adsorbed on the Ag, Au, and Cu Electrode Surfaces

assignment ^a	RS	wavenumbers/cm ⁻¹		
		Ag (-0.400 V)	Au (-0.400 V)	Cu (-0.600 V)
$\nu(\text{N}-\text{H})_{\text{amide}}$	3278	—	—	—
F2 [$\nu(=\text{C}-\text{H})$]	3063	3056	3056	3064
$\nu(\text{C}-\text{H})_{\text{aliphatic}}$	2979	—	—	—
$\nu(\text{CH})$, $\nu_{\text{as}}(\text{CH}_3)$ and/or $\nu_{\text{as}}(\text{CH}_2)$	2932	2927	2921	2925
$\nu_{\text{s}}(\text{CH}_2)$	2876	2874	2871	2876
$\nu(\text{C}-\text{H})$	—	2820 ^b	—	—
AI unordered	1672	1672	1671	1663 (1659) ^c
$\delta_{\text{as}}(\text{NH}_2)$ and/or W1 [indole + $\nu(\text{N}_1-\text{C}_8)$]	1621	1636	—	—
F8a	1606	1605	1603	1603 (1604)
F8b	1585	1582	1582	1584
W3 [pyrrole $\nu(\text{C}_2=\text{C}_3)$]	1552	1550	1551	1550 (1546)
disubstituted aromatic ring, Q [$\nu(\text{Im})$]	1493	1492	1494	1494 (1483)
$\delta(\text{CH}_2)$ and/or W5/F19a	1458	—	—	—
$\rho_{\text{s}}(\text{C}_\beta\text{H}_2)_{\text{F},\text{W}}$ and/or $\delta(\text{CH}_2)$	1435	1442	1437	1434 (1384)
W7 [pyrrole $\nu(\text{N}_1-\text{C}_8)$ + oop bending; Fermi resonance], Q, and/or $\rho_{\text{w}}(\text{CH}_2)$	1362	1380	1369	—
W7 [pyrrole $\nu(\text{N}_1-\text{C}_8)$; Fermi resonance], and/or $\rho_{\text{w}}(\text{CH}_2)$	1339	—	—	1343 (1335)
$\delta(\text{C}_\beta\text{H}_2)_{\text{F},\text{W}}$ and/or W8 [$\nu(\text{C}_3-\text{C}_9)+\delta(\text{N}_1\text{H})$]	—	—	1313	1314
Q [$\beta(\text{CH})$]	1287 ^{sh}	—	—	—
Am-III disordered and/or $\delta(\text{CC}_\alpha\text{H})$	1263	1267	1263	1267 (963) ^d
W10 [$\nu(\text{C}_3-\text{C}_\beta\text{H}_2)$ + $\nu(\text{C}-\text{H})$], Q [$\beta(\text{CH})/\nu(\text{Im})$]	1232	1242	1242	1234
F7a	1206	1205	1206	1205 (1205)
$\nu_{\text{as}}(\text{CCN})$ and/or $\rho_{\text{t}}(\text{NH}_2)$	1158	1142	1140	—
$\nu(\text{C}-\text{C})_{\text{T}}$ alkyl chain and/or $\rho_{\text{b}}(\text{CH})_{\text{W},\text{F}}$	1128	1111	1125	1109 (1106)
$\nu(\text{C}-\text{C})$ alkyl chain	1081	1074	—	1085
F18a	1032	1029	1027	1032 (1032)
W16 [phenyl and pyrrole rings out-of-phase breathing]	1012	1012 ^{sh}	1012 ^{sh}	1012 ^{sh}
F12	1004	1003	1003	1003 (1003)
$\nu(\text{C}-\text{C})$ and/or $\nu(\text{C}-\text{N})$	901	—	—	—
W17 [$\delta(\text{N}_1-\text{H})$ and Fermi resonance between phenyl ring breathing and o.o.p ring bend overtone]	879	—	878	879 (856)
$\nu(\text{C}-\text{C})$, $\nu_{\text{s}}(\text{CNC})$ secondary amide, and/or $\rho(\text{CH}_2)$	837	828	841	829
W18 [phenyl/pyrrole in-phase ring breathing]	758	757	759	758 (754)
$\nu(\text{C}-\text{S}) \text{ P}_{\text{C}}\text{-T}$	724	700	—	681
$\rho(\text{CH}_2)$	699	—	—	—
F6b	622	622	621	621 (621)
Am-VI	572	—	—	—

^a Abbreviations: W, F, and Q – tryptophane, phenylalanine, and histidine, respectively; Im – imidazole ring; Am – amide vibration; ν – stretching; ν_{s} – stretching symmetric; δ – deformation, δ_{as} – asymmetric deformation, ρ_{w} – wagging, ρ_{r} – rocking, and β – in-plane C–H ring deformation vibrations; T – trans conformation. ^b Determined at -1.200 V. ^c Data from spectrum in D₂O solution are presented in parentheses. ^d Determined from the SERS spectrum at the Ag electrode at 0.100 V in D₂O.

will be discussed below. It should be noted that the analysis of the bands in the 1580–1645 cm⁻¹ spectral region is not straightforward, because some contribution from the carbon contamination might take place, especially in the case of the Au and Ag electrodes (Figure S1, Supporting Information).

SERS Spectra of NMB Adsorbed on a Ag Electrode Surface. The SERS spectra of NMB adsorbed on the Ag electrode surface at different applied electrode potentials are shown in Figure 2. As is seen, at sufficiently negative electrode potential (-1.200 V), the relative intensity of the F12 mode due to the ring breathing

Table 2. Wavenumbers and fwhm of the F12 Mode in the SERS Spectra of NMB Adsorbed on the Ag, Au, and Cu Electrode Surfaces

electrode potential (V)	wavenumbers/cm ⁻¹		
	Ag	Au	Cu
-1.200	1000 (11) ^a	1003 (8)	-
-1.000	1001 (12)	1003 (7)	1003 (6)
-0.800	1001 (11)	1002 (7)	1003 (6)
-0.600	1002 (8)	1003 (7)	1003 (6)
-0.400	1003 (7)	1003 (7)	1003 (6)
+0.200	1003 (7)	1003 (8)	-

^a The fwhm values (cm⁻¹) are presented in parentheses.

vibration of the Phe⁹ residue was reduced and red-shifted in wavenumber by 4 cm⁻¹ to 1000 cm⁻¹ in comparison to those in the ordinary Raman spectrum of NMB. Also, the bandwidth of this mode, determined as the full width at half-maximum (fwhm), was broadened from 6 cm⁻¹ in the NMB Raman spectrum to 11 cm⁻¹ in the SERS spectrum (Table 2). These spectral changes point to the direct Phe⁹···Ag interaction and an end-on orientation of the Phe⁹ ring with respect to the Ag electrode surface. A weak relative intensity of a 3055 cm⁻¹ spectral feature due to the F2 mode (aromatic ν(=C—H)) supports the proposed tilted orientation of the Phe⁹ ring.³⁴ In the fingerprint spectral region, the relative intensity of the Amide-III mode at 1261 cm⁻¹ (α-helical secondary structure) increased and became equal to that of the F12 mode (Figure 2A, trace a). The high relative intensity of this mode suggests involvement of the amide bond in the NMB interaction with the Ag electrode surface at the negative electrode potential. The presence of the Amide-I band near 1670 cm⁻¹ (random coil conformation) and a 1132 cm⁻¹ spectral feature due to the antisymmetric stretching vibration of the C—C—N group^{35,36} support this hypothesis. Alternatively, the latter SERS signal could arise from the asparagine side-chain vibrations (Asn²). This is in agreement with the enhancement of the δ_{as}(NH₂) mode of Asn² that was masked by an “envelope” of overlapping bands in the spectral range of 1600–1645 cm⁻¹. Notably, the W16 (shoulder at 1009 cm⁻¹; based on an internally consistent deconvolution analysis) and W18 (757 cm⁻¹) modes due to the indole ring motions of Trp⁴ exhibited rather low relative intensities in the NMB SERS spectrum at -1.200 V (Figure 2A, trace a). The W18 mode at 757 cm⁻¹ was substantially broadened (fwhm = 35 cm⁻¹) as compared with that in the NMB Raman spectrum (fwhm = 9 cm⁻¹). On the other hand, the W7 mode (1361 cm⁻¹) produced an uncommonly strong and broad (fwhm = 29 cm⁻¹) SERS signal, which was symmetric in shape. Thus, we believe that these bands are a consequence of the Trp⁴···Ag interaction. Moreover, these bands may be interpreted as an unequivocal signal of the end-on close to flat orientation of the Trp⁴ indole ring with respect to the Ag electrode surface, because this arrangement would allow the lone electron pairs on the indole nitrogen atom to interact strongly with this surface. Another noteworthy contribution at 707 cm⁻¹ (fwhm = 16 cm⁻¹) in the NMB SERS spectrum at -1.200 V is due to the ν(C—S) band of Met¹⁰. It was red-shifted by 17 cm⁻¹ in comparison to its position in the spectrum of the nonadsorbed species, indicating that the methionine's C—S group was involved in the interaction with the Ag electrode surface at sufficiently negative electrode potential.

The high-frequency spectral region also provides evidence on the direct contact of the C—H bonds with the Ag electrode surface. A shoulder at 2820 cm⁻¹ in the SERS spectrum of NMB adsorbed at the Ag electrode surface at -1.200 V (Figure 2B) was attributed to the ν(C—H) vibrations of the —CH₂— groups being in direct contact with the metal surface.³⁷ When the electrode potential was polarized to less negative values (-0.400 V (Figure 2B, trace c) and 0.100 V (Figure 2B, trace d)), the ν(C—H) mode disappeared, indicating detachment of the corresponding molecular groups from the Ag electrode surface. At the same time, the F12 mode was strengthened and blue-shifted to its Raman value (ca. 1003 cm⁻¹) (Figure 2A, traces c and d; Table 2). The changes for F12 indicated that the Phe⁹ ring stands from the tilted arrangement to the close to perpendicular arrangement with respect to the Ag electrode surface. It is well-known that the F12 mode of the aromatic ring gains SERS enhancement when it adopts the vertical orientation at the Ag surface, when compared to that for the horizontal orientation.^{34,38} For the above-assumed alternations in the Phe⁹ orientation, the F2 mode (at 3055 cm⁻¹) involves large polarizability changes in the direction of the surface normal, which explains the observed increase in the relative intensity of this mode when the applied electrode potential becomes more positive.^{34,38} On the other hand, the relative intensities of the Amide-III, ν_{as}(CCN), W16, W18, W7, and ν(C—S) bands (see Table 1 for detailed wavenumbers and band assignment) appear to decrease when the applied electrode potential becomes more positive (-0.400 and 0.100 V) (Figure 2A, traces c and d). Hence, we may infer that together with the increase of the electrode positive charge, the —CONH— bond and the Asn², Trp⁴, and Met¹⁰ residues were more distant from the Ag electrode surface. However, because the signal-to-noise ratio for the SERS spectra presented here was not large enough to allow conclusions about the subtle changes in the enhancement of the W16, W18, and ν(C—S) SERS signals, we performed G2DCA to test the above statement. The G2D correlation method usually allows both the ability to distinguish intensity changes that are not sufficiently pronounced to be observed using simple spectral analysis, and increasing separation of the overlapping components present within the broad band envelope. This method is useful in the analysis of spectral signals, which change as a function of many kinds of physical variables affecting the spectra, such as time, temperature, concentration, potential, pressure, and even chemical reaction.^{19,39,40} Figure 5 presents (A,C) synchronous and (B,D) asynchronous G2D-correlation maps in the frequency ranges of 950–1550 and 2800–3100 cm⁻¹ generated, using variations of the electrode potential as a variable, from the SERS spectra of NMB adsorbed on the Ag electrode surface. The synchronous G2D-correlation maps contain two very strong (at (1003,1003) (Figure 5A) and (2927,2927) cm⁻¹ (Figure 5C)), three medium (at (1267,1267), (1362,1362), and (1390,1390) cm⁻¹ (Figure 5A)), and four low intensity (at (1029,1029), (1132,1132), (1242,1242) (Figure 5A), and (3058,3058) cm⁻¹ (Figure 5C)) autopeaks. The strong intensity of the (1003,1003) and (2927,2927) cm⁻¹ peaks suggest that the enhancement of these band was changed most significantly with the change of the Ag electrode potential. However, there are no peaks located at the diagonal positions that represent the 1009 (W16), 757 (W18), and 707 cm⁻¹ (ν(S—C)) SERS signals (Figure 5A). This leads to the conclusion that there is no relative intensity alternation of these bands for the Ag electrode potentials between -1.200 and 0.100 V. Hence,

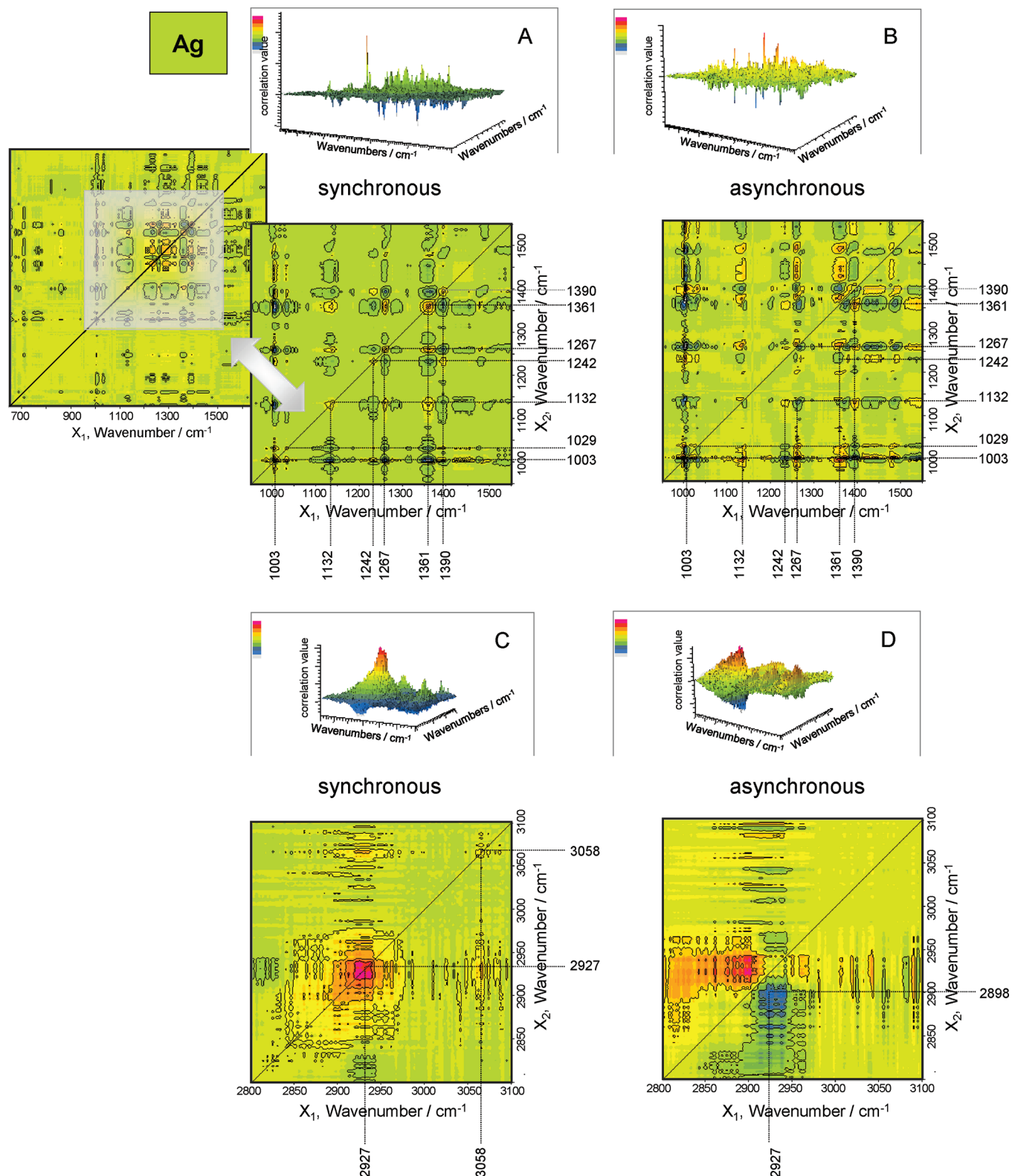


Figure 5. Generalized synchronous (A,C) and asynchronous (B,D) 2D-correlation maps of SERS spectra of NMB adsorbed on a Ag electrode surface as a function of electrode potential; spectral ranges of 950–1550 and 2800–3100 cm⁻¹.

there is no difference between the indole ring π -electrons system and the S–C bond in the strength of interaction with the Ag electrode surface when the electrode potential becomes more positive. These observations provide clear evidence that there

was no potential-induced variation in the orientation of the Trp⁴ and Met¹⁰ residues with respect to the Ag electrode surface and disproves the statement proposed earlier for Trp⁴ and Met¹⁰ based on the visual analysis. In addition to the autopaks, several

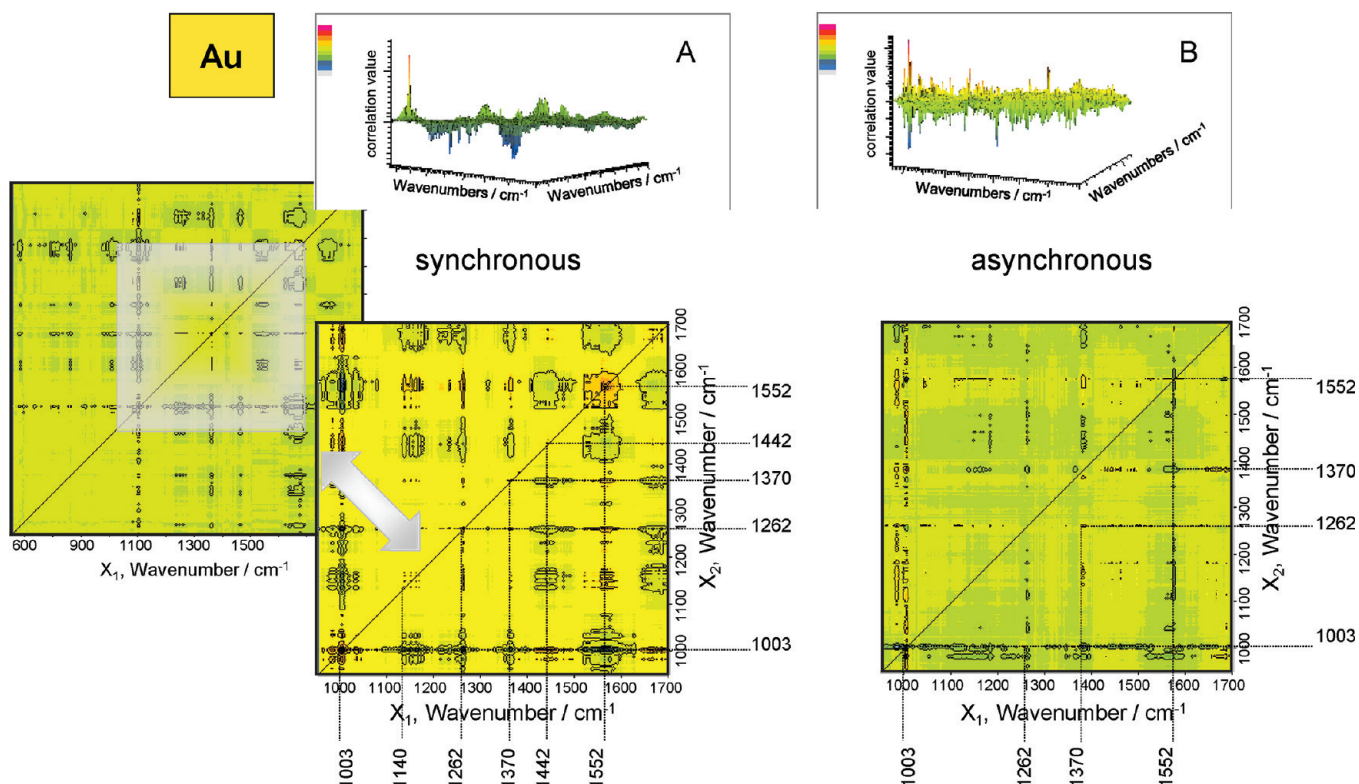


Figure 6. Generalized synchronous (A) and asynchronous (B) 2D-correlation maps of SERS spectra of NMB adsorbed on a Au electrode surface as a function of electrode potential; spectral range of 950–1700 cm⁻¹.

positive cross-peaks at (1361,1267), (1361,1132), (1267,1132), (1029,1003), and (3058,2927) cm⁻¹ are present in the synchronous G2D-correlation maps (Figure 5A,C). The positive sign of these cross-peaks indicates that all these SERS signals underwent potential-dependent enhancement changes in the same direction. By contrast, the negative sign of the (1132,1003), (1267,1003), (1361,1003), (1390,1267), and (1390,1361) cm⁻¹ cross-peaks informs about enhancement changes in the reverse direction. Also, the asynchronous G2D-correlation maps develop several cross-peaks (Figure 5B,D). The appearance of these peaks suggests that the directions of the transition moments of these modes were different. The positive sign of the (1267,1003), (1361,1003), (1132,1003), (1390,1267), (1390,1361), and (3058,2927) cm⁻¹ peaks indicates that potential-induced spectral changes took place earlier at 1267, 1361, and 1132 cm⁻¹ than that at 1003 cm⁻¹. Similarly, those at 1267 and 1361 cm⁻¹ followed the former at 1390 cm⁻¹, and the latter at 3058 cm⁻¹ overreached that at 2927 cm⁻¹. On the other hand, the negative sign of the two example peaks at (1267,1132) and (1361,1132) cm⁻¹ suggests that spectral alternations took place earlier at 1132 cm⁻¹ than those at 1267 and 1361 cm⁻¹. Summarizing, when the applied electrode potential becomes less negative, at first the rearrangement of the Asn² side-chain was observed. It then flipped, so that the –CCN– fragment descended the Ag electrode surface, while the C=O unit approached this surface. This switch weakened the Trp⁴H–N₈···Ag and COHN···Ag interactions. Finally, these alternations produced gain in the relative intensities of the F12, F18a, and F2 modes (A₁ symmetry, assuming the C_{2v} point symmetry group of adsorbed Phe⁹) as a consequence of the Phe⁹ ring standing on the Ag electrode surface.

SERS Spectra of NMB Adsorbed on a Au Electrode Surface.

In the case of the adsorption process of NMB on the Au electrode surface (Figure 3), no shift in wavenumber and small width broadening ($\Delta_{\text{fwhm}} = 3$ cm⁻¹) of the F12 mode (1003 cm⁻¹) were observed between the SERS and Raman spectra (see Table 1). The position and width of this band were unchanged when the Au electrode potential became more positive (up to 0.200 V), while its relative intensity was significantly raised when the Au electrode potential was changed from -1.200 V to -0.800 V. The enhancement and magnitude of the enhancement growth was comparable to those observed for NMB on the Ag electrode surface at the same potential range. Further increase in the applied Au electrode potential did not strengthen this band enhancement. Thus, at -1.200 and -0.800 V the Phe⁹ ring on the Au electrode surface adopted orientations similar to those on the Ag electrode surface at the same applied electrode potentials, and the latter did not change the arrangement with continued increase in the Au electrode potential. Without doubt, other changes in the NMB SERS profile on the Au electrode surface were not as distinct as that of the 1003 cm⁻¹ band and required the use of G2DCA for the proper analysis. Thus, on going from the SERS spectra (Figure 2) and G2D-correlation maps (Figure 5) of NMB adsorbed on the Ag electrode surface to the SERS spectra (Figure 3) and G2D-correlation maps (Figure 6) of this neurotransmitter immobilized on the Au electrode surface, several important similarities in the relative intensity of the discussed spectral features were observed. For example, the most intense autopeaks of the synchronous G2D-correlation map (Figure 6A) were (1003,1003) and (1262,1262) cm⁻¹, while three remaining autopeaks at (1370,1370) and (1140,1140) cm⁻¹ were weak. This means that the 1003 and 1262 cm⁻¹ SERS signal enhancements

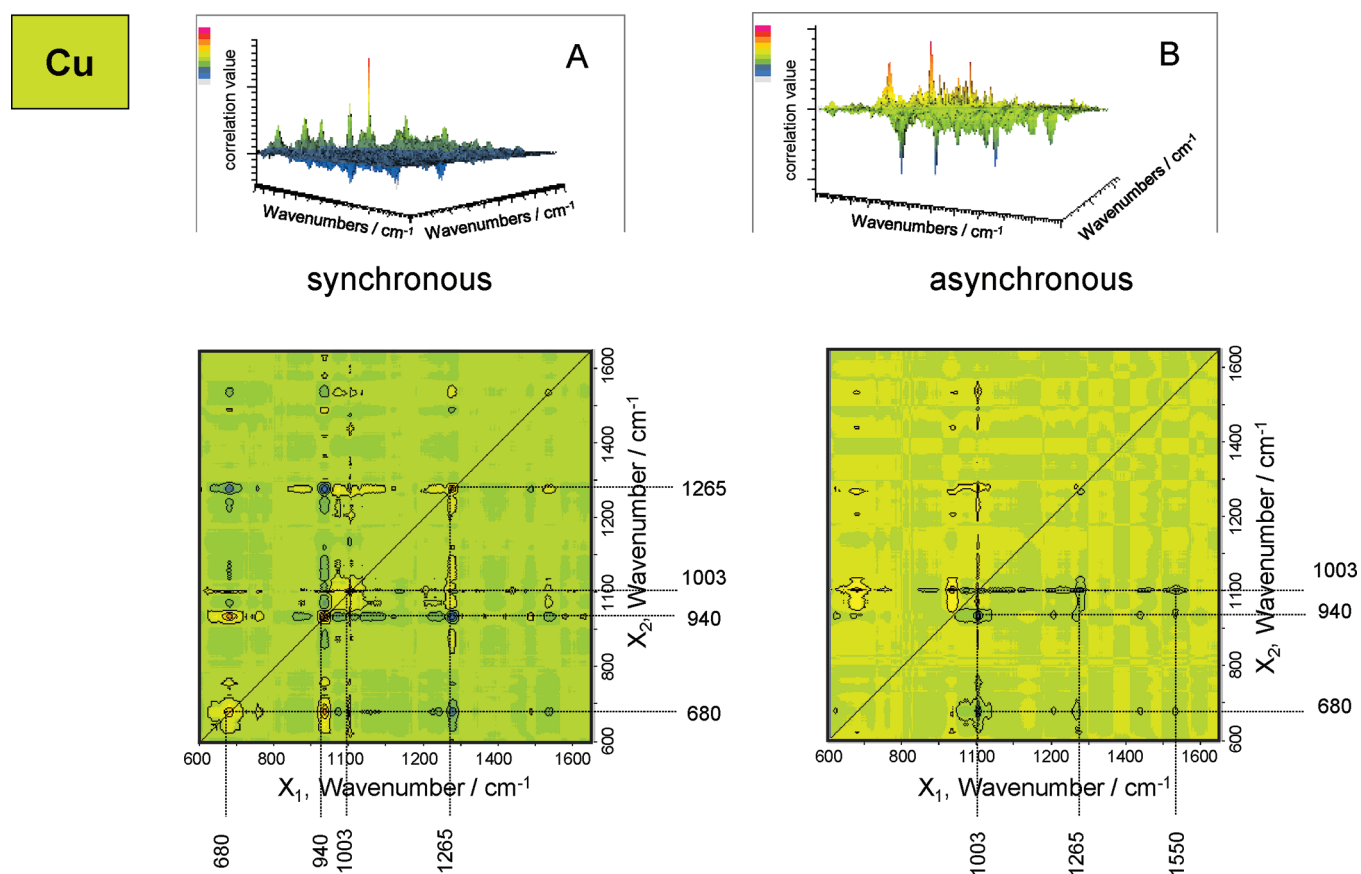


Figure 7. Generalized synchronous (A) and asynchronous (B) 2D-correlation maps of SERS spectra of NMB adsorbed on a Cu electrode surface as a function of electrode potential; spectral range of 600–1700 cm^{-1} .

on both the Au and Ag electrode surfaces were prominently changed, whereas for the 1369 and 1140 cm^{-1} spectral features the observed variations were small. On the other hand, the (1552,1552) (strong) and (1442,1442) cm^{-1} (weak) autopeaks (Figure 6A) (see Table 1 for detailed band assignments) drew distinctions between the potential-induced changes in the NMB adsorption on the Au and Ag electrode surfaces, because they are not present in the NMB synchronous G2D-correlation map on the Ag electrode surface (Figure 5A). Note also that the autopeaks of the synchronous G2D-correlation map on Ag (Figure 5A,C) assignable to $\nu(\text{C=O})$, F18a, W10, and F2 (see Table 1 for band positions) disappeared in the synchronous G2D-correlation map of NMB deposited on the Au electrode (Figure 6A). These facts show that slightly different changes in the NMB structure occur on the Au electrode surface when this electrode potential becomes more positive than those on Ag. Also, two distinct positive, i.e., (1442,1003) and (1552,1262) cm^{-1} , and three negative, i.e., (1552,1003), (1262,1003), and (1370,1003) cm^{-1} , cross-peaks were observed (Figure 6A), suggesting that the relative intensities of these spectral features were altered in the same and reverse directions, respectively. On the other hand, from the asynchronous G2D-correlation map of NMB on the Au electrode surface (Figure 6B), it is evident that the change at 1003 cm^{-1} took place earlier than that at 1369 cm^{-1} , which went before that at 1262 cm^{-1} . These results highlight the following possible change in the adsorption mechanism of NMB on the Au electrode surface. At -1.200 V, the Phe⁹ ring adopted tilted orientation with respect to the Au electrode surface, similar to that

on the Ag electrode surface. When the Au electrode potential reached -0.800 V, the tilt angle that formed between the Phe⁹ ring and the Au substrate was increased and stayed invariant during continuing increase of the positive charge of the electrode. This was observed as an initial intensification of the 1003 and 1442 cm^{-1} SERS signals ($I_{1003} \uparrow$ and $I_{1442} \uparrow$). Within this early reorientation, the lone pair of electrons on the indole nitrogen atom was only slightly depressed in contact with the Au electrode surface ($I_{1370} \downarrow$), which further caused the weakening of the indole C₂=C₃ and CONH bond interactions with this surface ($I_{1552} \downarrow$ and $I_{1262} \downarrow$). It should be also stressed that only negligible changes in the CCN \cdots Au interaction were detected when the Au electrode potential became more positive. This means that the reorientation of the Asn² side-chain did not occur as took place in the case of NMB immobilization onto the Ag electrode surface. Thus, the $\nu(\text{C=O})$ mode was absent in the NMB SERS spectra on the Au electrode surface. Another marked difference between these two electrode surfaces was the lack of both the $\nu(\text{C-S})$ mode, pointing out that the methionine side-chain was not involved in the coordination to the Au electrode surface and the changes in the high frequency region (2800–3100 cm^{-1}) during changes in the electrode potential. Therefore we omitted the G2D-correlation maps in this spectral range.

SERS Spectra of NMB Adsorbed on a Cu Electrode Surface. The SERS pattern of NMB deposited onto the Cu electrode surface (Figure 4) closely resembles those of this peptide deposited onto the Ag and Au electrode surfaces (Figures 2 and 3), except for the strong 940 cm^{-1} band (phosphate anions).

This similarity clearly points out that, in general, the same molecular fragments of NMB participated in the interactions with each of the metal electrodes. However, contrary to the Ag and Au electrode surfaces it seems that the relative intensities of the NMB SERS signals in these spectra at the different applied electrode potentials were identical, with the exception of the 1003 cm^{-1} (F12) spectral feature (Figure 4A). As is evident, at -1.200 V the enhancement of the 1003 cm^{-1} SERS signal was stronger than that on the Ag and Au electrode surfaces, suggesting that the Phe⁹ ring on the Cu electrode adopted a more vertical orientation than that on the Ag and Au electrodes at the same electrode potential. With continuing increase of the positive Cu electrode potential up to -0.400 V , F12 increases in relative intensity comparable to that in the NMB Raman spectrum. Hence, the Phe⁹ ring was nearly perpendicular with respect to the Cu electrode surface at -0.400 V . The relatively strong scattering at 3064 cm^{-1} confirms this statement (Figure 4B). The synchronous G2D-correlation map generated from these spectra (Figure 7A), showing two strong (at $(1003,1003)$ and $(940,940)\text{ cm}^{-1}$), one medium (at $(1265,1265)$ (Amide-III)), and one weak (at $(680,680)\text{ cm}^{-1}$ ($\nu(\text{C}-\text{S})$)) autopeaks, confirmed the results obtained for NMB adsorbed on the roughened Ag and Au electrodes. Also, they indicate that the most prominent changes in the NMB adsorption on the Ag, Au, and Cu electrodes were associated with the reorientation of the Phe⁹ ring and amide bond. However, both the $(1265,680)$ (negative) and $(1265,1003)\text{ cm}^{-1}$ (positive) cross-peaks in the synchronous G2D-correlation map (Figure 7A) and several negative cross-peaks, i.e., $(1003,680)$, $(1265,1003)$, and $(1550,1003)\text{ cm}^{-1}$, in the asynchronous G2D-correlation map (Figure 7B) provided evidence for a different sequence of the electrode potential-induced changes in the NMB adsorption on the Cu electrode surface versus the Ag and Au electrode surface. Briefly, using these maps we can conclude that the 1003 , 1265 , and 680 cm^{-1} SERS signals were increased in relative intensity when the electrode potential became less negative. Moreover, the alternation at 1003 cm^{-1} took place earlier than those at 1550 and 1265 cm^{-1} and later than that at 680 cm^{-1} . This information illustrates that when the electrode potential becomes more positive, the slight rearrangement of the Met¹⁰ C–S bond on the Cu electrode surface initiated the successive changes in the orientation of the amide and Trp⁴ $\text{C}_2=\text{C}_3$ bonds and the Phe⁹ ring rearrangement on this surface.

Potential Dependence of Amide-III Band Wavenumber. As is well-established, the spectral regions, where the amide bond vibrations appear, are sensitive to changes in the peptide and protein secondary structures. However, the frequency correlation with proper secondary structure is challenging,^{41,42} especially in the Amide-III spectral region (1200 – 1300 cm^{-1}), where usually several strongly scattered bands due to different peptide fragment motions contribute the spectra.^{43,44} Thus, we performed detailed analysis in this spectral range. Figure 8 presents results of the H₂O/D₂O solvent exchange experiment for NMB immobilized onto the Cu electrode surface at an applied electrode potential of -0.600 V . As is seen, the 1267 cm^{-1} band in H₂O disappears in the D₂O spectrum. Unfortunately, a strong band near 938 – 943 cm^{-1} due to the adsorbed phosphate anions prohibited more detailed examination of this spectral region in D₂O for the Cu electrode. However, analysis of the SERS of NMB immobilized onto the Ag electrode in D₂O revealed a new SERS band at ca. 963 cm^{-1} (Table 1). This was a consequence of NH/ND exchange and proved the assignment of this band to the Amide-III mode. Figure 9 shows

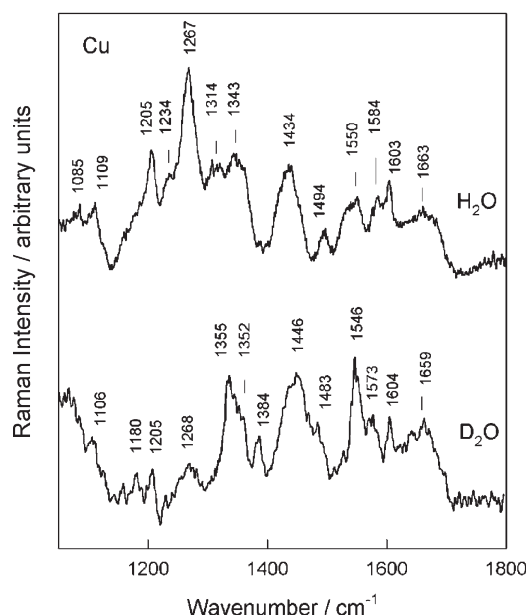


Figure 8. SERS spectra of NMB adsorbed on roughened Cu electrode at -0.600 V in H₂O and D₂O. Measurement conditions: 10^{-5} M NMB in 0.1 M Na₂SO₄ solution containing 0.01 M phosphate buffer (pH 7.0); excitation wavelength, 785 nm; laser power at the sample, 50 mW; integration time, 300 s. Spectra were normalized to the F12 mode.

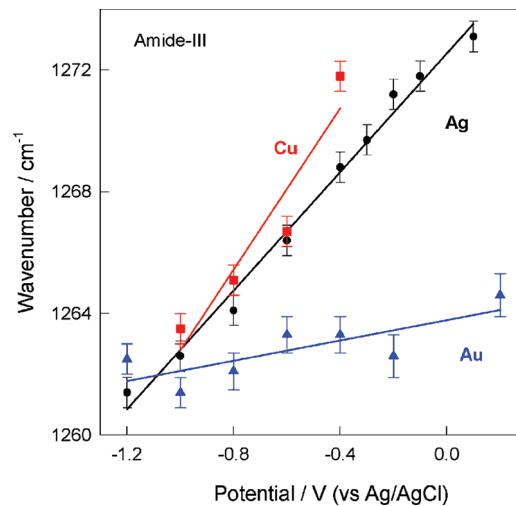


Figure 9. Scheme of potential-dependent shift in the Amide-III band wavenumber of NMB deposited onto Ag, Au, and Cu electrode surfaces. Solid lines indicate linear regression fits.

the potential-dependent alternations in the Amide-III band wavenumber obtained by fitting of the SERS spectra of NMB deposited onto the Ag, Au, and Cu electrodes using the mixed Gaussian–Lorentzian functions. The obtained dependence was nearly linear with slope, $d\nu(\text{Am-III})/dE$, highly sensitive to the nature of the electrode type (equal to 13.3, 9.7, and $1.7\text{ cm}^{-1}/\text{V}$ for the Cu, Ag, and Au electrodes, respectively). The band frequencies were lower at the more negative electrode potentials than those at the more positive electrode potentials, yielding positive $d\nu(\text{Am-III})/dE$ values. Observed Amide-III frequency–potential dependencies demonstrate the presence of the electrochemical Stark effect, which is associated with modulation

of vibrational force constants of the amide group by the potential drop at the interface.^{45–47} Such an effect can originate from several sources, including pure electrostatic influence on a particular vibration,⁴⁶ modifications of adsorbate–surface bonding,^{45,47} and modification of hydrogen bonding strength of the amide group with water molecules or neighboring peptides. The observed downshift of the Amide-III frequency at more negative potentials is characteristic of the weakening of hydrogen bonding between the water molecules and the amide C=O and N–H groups observed in the temperature-dependent experiments for peptides dissolved in water.^{42,48} The mechanism of this effect was explained by the hydrogen-bonding-induced stabilization of one of the resonance structures.^{48–50} Briefly, the strong hydrogen bonding stabilizes the resonance form with the C–O and C=N amide bonds. A temperature increase weakens this hydrogen bonding, and resonance with the C=O and C–N amide bonds becomes more pronounced, resulting in the Amide-III and Amide-II band frequencies lowering and increasing of the Amide-I band wavenumber. Also, the strong hydrogen bonding increases the N–H bending force constant, resulting in the Amide-II and Amide-III bands frequency upshift.⁵¹ Based on these, it could be presumed that a similar mechanism takes place for NMB adsorbed on the Ag, Au, and Cu electrode surfaces. However, the strong interaction of –CONH– with a metal is only possible when the deprotonation of the nitrogen atom occurs.^{52,53} This process is usually demonstrated by an intense ca. 1420 cm⁻¹ Raman band due to the in-phase stretching vibration of the C=O/C–N⁻ bonds.⁵² Such a spectral feature was not observed in this work. Thus, the observed shift in wavenumber of the Amide-III band might be associated with the potential-induced modulation of the hydrogen bonding strength of the amide group due to the changes in the interfacial water structure or to the conformational changes in the hydrogen bond formed between neighboring peptides. Differences in the wavenumber-potential dependence slots for the three studied coinage metals can be associated with the different positions of the potential of zero charge (pzc) for studied electrodes. Because the pzc of the Ag electrode in the surface-inactive electrolytes (−0.90 V) is about 1 V more negative compared with Au (0.0–0.10 V),^{54,55} the surface of the Ag electrode was positively charged in the majority of the studied potential region, while the Au electrode was negatively charged. Cu has pzc values similar to those of Ag.⁵⁶ Consequently, the orientation of the peptide group may be different, resulting in distinctly higher slopes determined for the Ag (13.3 cm⁻¹/V) and Cu (9.7 cm⁻¹/V) electrodes compared with Au (1.7 cm⁻¹/V). Recently, the different Stark-tuning slopes (dν/dE) of the CN group for 2-amino-4-cyanopyridine adsorbed on the Au electrode were explained by the reorientation of adsorbate.⁵⁷

Evidence for His Interaction with Cu Electrode Surface. His⁸ imidazole nitrogens (N_{π} and N_{τ}) are important binding sites of metal ions. In an aqueous solution, at physiological pH, only one of these nitrogen atoms is protonated. The position of the protonation defines the imidazole tautomeric form (N_{π} –H or N_{τ} –H). The N_{τ} –H form was found to be the more stable tautomer compared to N_{π} –H.⁵⁸ Raman spectroscopy distinguishes both the metal ion-bonded and free His and also its different tautomeric forms.^{52,59} Interaction of the imidazole ring with the Au,⁶⁰ Cu,⁶¹ and Ag⁶² surfaces at certain conditions has been also proven by the SERS technique. Unfortunately, Raman scattering of the His side-chain is relatively weak and overlaps with the other spectral features, particularly in the presence of the

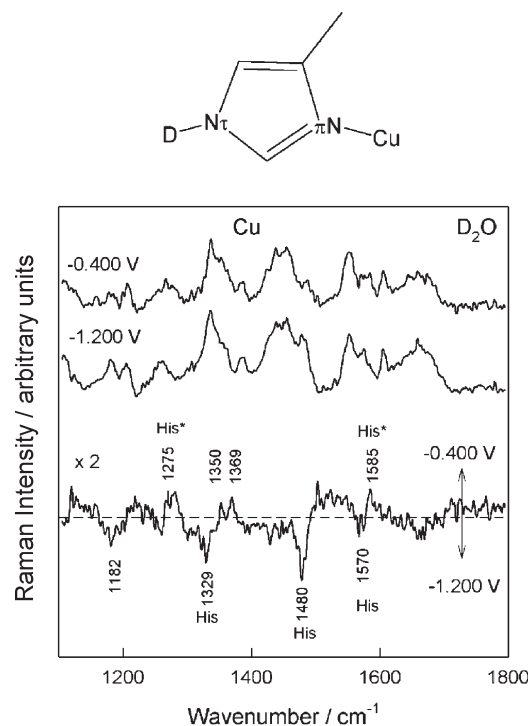


Figure 10. SERS spectra of NMB adsorbed on a Cu electrode at −0.400 and −1.200 V electrode potentials in D₂O and their difference spectrum. Measurement conditions: 10⁻⁵ M NMB in 0.1 M Na₂SO₄ solution containing 0.01 M phosphate buffer (pH 7.0). His and His* indicate free and Cu surface-bonded His⁸, respectively. The structure of the surface-bonded His⁸ is shown on top. Spectra were normalized to the F12 mode.

Phe and Trp residues. Therefore, in order to prove possible involvement of His⁸ in the interaction with the Cu electrode surface, we calculated a potential-difference spectrum. Thus, Figure 10 shows the SERS spectra of NMB deposited onto the Cu electrode surface at applied electrode potential of −0.400 and −1.200 V in the His fingerprint region and the corresponding difference spectrum. In order to avoid the strong influence of the ca. 1267 cm⁻¹ SERS signal, which overlaps with the His⁸ ring breathing mode, the data were obtained in D₂O. The difference spectrum shows subtle potential-induced spectral changes (Figure 10, bottom trace). Briefly, a negative 1570 cm⁻¹ band was due to the C₄=C₅ stretching vibration of the His⁸ ring.^{52,63,64} Unfortunately, it can not be used to distinguish between two imidazole tautomeric forms (His(N_{π}))–metal exhibits slightly higher frequency than that of His(N_{τ}))–metal). This is because in D₂O the sensitivity of this mode disappears.⁵² A positive 1585 cm⁻¹ spectral feature pointed to the His⁸ ring···Cu coordination at the less negative electrode potential (see Table 1 for band assignment). A positive broad ca. 1275 cm⁻¹ band served as the second marker of the imidazole ring coordination to the Cu electrode surface.⁵² Its intensification was characteristic for the His(N_{π}))–metal coordination^{52,64} and indicated an increase in its enhancement at less negative applied electrode potential (−0.400 V). The third signature of the His⁸ ring···Cu bonding was a negative signal at ca. 1480 cm⁻¹ due to the imidazole ring stretching vibrations.⁶⁵ Since, it is known that the 1480 cm⁻¹ band characteristic for the unbound N-deuterated histidine residue decreases in relative intensity upon imidazole ring coordination to Cu(II),⁵³ the presented difference spectrum provides clear evidence for bonding of the His⁸ ring to

the Cu electrode surface at relatively positive electrode potentials (-0.400 V). Additionally, the intensification of the imidazole ring breathing mode suggests that the coordination to the Cu surface takes place through the N_{π} atom.

CONCLUSIONS

The presented results demonstrate the feasibility of the combination of SERS, electrochemistry, solvent isotopic exchange, and G2DCA methods in determination of the adsorption mechanism, orientation with respect to a metal surface, and even small alterations in this orientation upon the change of the applied electrode potential for NMB in an aqueous buffered solution (pH = 7.0).

Based on the obtained data we made the following conclusions:

- I. The SERS spectra demonstrated that NMB deposited onto the Ag, Au, and Cu electrode surfaces show bands due to vibrations of the moieties that were in contact/close proximity to the electrode surfaces and thus should be located on the same side of the polypeptide backbone. These include the Phe⁹ and Trp⁴ rings, the sulfur atom of Met¹⁰, the $-\text{CCN}-$ and $-\text{C=O}$ units of Asn², and His⁸. As is evident from Figure 1, the aforementioned positions in the NMB sequence fit these requirements.
- II. NMB adsorbed on the Ag electrode surface. When the applied electrode potential becomes less negative, at first the rearrangement of the Asn² side-chain was observed. It then flipped, so that the $-\text{CCN}-$ fragment descended the Ag electrode surface, while the C=O unit approached this surface. This switch weakened the Trp⁴ H–N₈ \cdots Ag and COHN \cdots Ag interactions. Finally, these alternations produced gain in the enhancement of the F12, F18a, and F2 modes as a consequence of the Phe⁹ ring standing on the Ag electrode surface.
- III. NMB adsorbed on the Au electrode surface. At negative electrode potential, the Phe⁹ ring adopted an end-on orientation with respect to the electrode surface, similar to the Ag electrode. At an electrode potential of -0.800 V, a tilt angle formed between the Phe⁹ ring, and the electrode surface was increased and stayed invariant during continuing increase of the positive charge of the electrode. Within this early reorientation, the lone pair of electrons on the indole nitrogen atom was only slightly depressed in contact with the Au electrode surface, which further caused the weakening of the indole C₂=C₃ and CONH bonds interactions with this surface. Only negligible changes in the CCN \cdots Au interaction were detected. This means that the reorientation of the Asn² side-chain did not occur as took place in the case of NMB immobilization onto the Ag electrode surface. Thus, the $\nu(\text{C=O})$ mode was absent in the NMB SERS spectra on the Au electrode. Another marked difference between these two electrode surfaces was the lack of both $\nu(\text{C-S})$ modes, indicating that the methionine side-chain was not involved in the coordination to the Au electrode surface.
- IV. NMB adsorbed on the Cu electrode surface. When the electrode potential became more positive, the slight rearrangement of the Met¹⁰ C–S bond on the Cu electrode surface initiated successive changes in the orientation of the amide and Trp⁴ C₂=C₃ bonds and the Phe⁹ ring rearrangement on this surface.
- V. The potential-difference SERS spectrum of NMB in D₂O adsorbed on the Cu electrode surface proved that the N_π atom of the His⁸ imidazole ring was bonded to the Cu electrode surface at relatively positive electrode potential.
- VI. The potential-induced modulation of the hydrogen bonding interaction strength at the interfaces was shown by the linear dependence of the Amide-III band wavenumber on the applied electrode potential (electrochemical Stark effect). The frequency–potential slope, $d\nu(\text{Am-III})/dE$, was dependent on the nature of the electrode and decreased in the following order: Cu ($13.3 \text{ cm}^{-1}/\text{V}$) > Ag ($9.7 \text{ cm}^{-1}/\text{V}$) \gg Au ($1.7 \text{ cm}^{-1}/\text{V}$).

The differences in the potential-dependence on the three surfaces (Cu, Ag, Au) are due to the variations in the Fermi level of the three metals (see Figures 9 and 10 of ref 66). Therefore, at a given wavelength, the ratio of the nontotally symmetric bands (such as 2927 cm^{-1}) to the symmetric bands (such as 2874 cm^{-1}) has a maximum (with respect to potential) that varies with the Fermi Level of the metal. Other examples are, for example, the ratio of the F8b to F8a modes. These illustrate the charge-transfer contributions to the SERS spectrum. Unfortunately, presented spectra were so dense that the quantitative measurements of the line intensities were difficult. However, these trends are clear by visual observation, and they coincide with the analysis of the above paper.

ASSOCIATED CONTENT

S Supporting Information. Comparison of SERS spectra before and after adsorption of NMB (Figure S1). This material is available free of charge via the Internet at <http://pubs.acs.org>.

AUTHOR INFORMATION

Corresponding Author

*E-mail: (E.P.) podstawk@chemia.uj.edu.pl; (G.N.) gniaura@ktl.mii.lt.

ACKNOWLEDGMENT

This work was supported by the State Department for Scientific Research of the Ministry of Science and Higher Education (Grant No. N N204 159136 to E.P.). I. Ignatjev acknowledges EU Structural Funds project “Postdoctoral Fellowship Implementation in Lithuania” for funding his postdoctoral fellowship. John Lombardi acknowledges the support of Award No. 2006-DN-BX-K034 by the National Institute of Justice, Office of Justice Programs, U.S. Department of Justice.

REFERENCES

- (1) Variola, F.; Bruski, J. B.; Orsini, G.; de Oliveira, P. T.; Wazen, R.; Nanci, A. *Nanoscale* **2011**, *3*, 335.
- (2) Heinz, H.; Farmer, B. L.; Pandey, R. B.; Slocik, J. M.; Patnaik, S. S.; Pachter, R.; Naik, R. R. *J. Am. Chem. Soc.* **2009**, *131*, 9704.
- (3) Sethi, M.; Pacardo, D. B.; Knecht, M. R. *Langmuir* **2010**, *26*, 15121.
- (4) Gray, J. J. *Curr. Opin. Struct. Biol.* **2004**, *14*, 110.
- (5) Minamino, N.; Kangawa, K.; Matsuo, H. *Biochem. Biophys. Res. Commun.* **1983**, *114*, 541.
- (6) Krane, I. M.; Naylor, S. L.; Helin-Davis, D.; Chin, W. W.; Spindel, E. R. *J. Biol. Chem.* **1988**, *263*, 13317.

- (7) Orbuch, M.; Taylor, J. E.; Coy, D. H.; Mrozinski, J. E., Jr.; Mantey, S. A.; Battey, J. F.; Moreau, J. P.; Jensen, R. T. *Mol. Pharmacol.* **1993**, *44*, 841.
- (8) Nock, B. A.; Nikolopoulou, A.; Galanis, A.; Cordopatis, P.; Waser, B.; Reubi, J. C.; Maina, T. *J. Med. Chem.* **2005**, *48*, 100.
- (9) Stiles, P. L.; Dieringer, J. A.; Shah, N. C.; Van Duyne, R. P. *Anal. Chem.* **2008**, *1*, 601.
- (10) Bell, S. E. J.; Sirimuthu, N. M. S. *Chem. Soc. Rev.* **2008**, *37*, 1012.
- (11) Kneipp, K.; Kneipp, H.; Itzkan, I.; Dasari, R. R.; Feld, M. S. *J. Phys.: Condens. Matter.* **2002**, *14*, R597.
- (12) Schlucker, S. *Chem. Phys. Chem.* **2009**, *10*, 1344.
- (13) Nabiev, I.; Chourpa, I.; Manfait, M. *J. Raman Spectrosc.* **1994**, *25*, 13.
- (14) Podstawka, E.; Ozaki, Y. *Biopolymers* **2008**, *89*, 807.
- (15) Podstawka, E.; Proniewicz, L. M. *J. Phys. Chem. B* **2009**, *113*, 4978.
- (16) Podstawka, E.; Ozaki, Y. *Biopolymers* **2008**, *89*, 941.
- (17) Podstawka, E.; Ozaki, Y.; Proniewicz, L. M. *Langmuir* **2008**, *24*, 10807.
- (18) Podstawka, E.; Niaura, G. *J. Phys. Chem. B* **2009**, *113*, 10974.
- (19) Podstawka, E.; Niaura, G.; Proniewicz, L. M. *J. Phys. Chem. B* **2010**, *114*, 1010.
- (20) Podstawka-Proniewicz, E.; Niaura, G.; Proniewicz, L. M. *J. Phys. Chem. B* **2010**, *114*, 5117.
- (21) Podstawka, E. *Biopolymers* **2008**, *89*, 506.
- (22) Podstawka, E. *J. Raman Spectrosc.* **2008**, *39*, 1290.
- (23) Podstawka, E. *Biopolymers* **2008**, *89*, 980.
- (24) Podstawka-Proniewicz, E.; Kudelski, A.; Kim, Y.; Proniewicz, L. M. *J. Phys. Chem. B* **2011**, *115*, 7079.
- (25) Podstawka-Proniewicz, E.; Kudelski, A.; Ozaki, Y.; Kim, Y.; Proniewicz, L. M. *J. Phys. Chem. A* **2011**, *115*, 6709.
- (26) Niaura, G.; Gaigalas, A. K.; Vilker, V. L. *J. Raman Spectrosc.* **1997**, *28*, 1009.
- (27) Bulovas, A.; Dirvianskyte, N.; Talaikyte, Z.; Niaura, G.; Valentukonyte, S.; Butkus, E.; Razumas, V. *J. Electroanal. Chem.* **2006**, *591*, 175.
- (28) Kazakevičienė, B.; Valincius, G.; Niaura, G.; Talaikytė, Z.; Kažemėkaitė, M.; Razumas, V. *J. Phys. Chem. B* **2003**, *107*, 6661.
- (29) Gao, P.; Gosztola, D.; Leung, L. W. H.; Weaver, M. J. *J. Electroanal. Chem.* **1987**, *233*, 211.
- (30) Roth, E.; Hope, G. A.; Schweinsberg, D. P.; Kiefer, W.; Fredericks, P. M. *Appl. Spectrosc.* **1993**, *47*, 1794.
- (31) Niaura, G.; Malinauskas, A. *Chem. Phys. Lett.* **1993**, *207*, 455.
- (32) Niaura, G.; Gaigalas, A. K.; Vilker, V. L. *J. Phys. Chem. B* **1997**, *101*, 9250.
- (33) Lee, S.; Kim, Y. *FEBS Lett.* **1990**, *460*, 263.
- (34) Gao, X.; Davies, J. P.; Weaver, M. J. *J. Phys. Chem.* **1990**, *94*, 6858.
- (35) Silva, B. L.; Freire, P. T. C.; Melo, F. E. A.; Guedes, I.; Silva, M. A. A.; Filho, J. M.; Moreno, A. J. D. *Braz. J. Phys.* **1998**, *28*, 19.
- (36) Herne, T. M.; Ahern, A. M.; Garrell, R. L. *J. Am. Chem. Soc.* **1991**, *113*, 846.
- (37) Razmuto-Razmė, I.; Kuodis, Z.; Eicher-Lorka, O.; Niaura, G. *Phys. Chem. Chem. Phys.* **2010**, *12*, 4564.
- (38) Moskovits, M.; Suh, J. S. *J. Phys. Chem.* **1988**, *92*, 6327.
- (39) Molenda, M.; Dziembaj, R.; Podstawka, E.; Proniewicz, L. M. *J. Phys. Chem. Solids* **2005**, *66*, 1761.
- (40) Buchet, R.; Wu, Y.; Lachenal, G.; Raimbault, C.; Ozaki, Y. *Appl. Spectrosc.* **2006**, *55*, 155.
- (41) Weymuth, T.; Jacob, C. R.; Reiher, M. *J. Phys. Chem. B* **2010**, *114*, 10649.
- (42) Mikhonin, A. V.; Ahmed, Z.; Ianoul, A.; Asher, S. A. *J. Phys. Chem. B* **2004**, *108*, 19020.
- (43) Asher, S. A.; Mikhonin, A. V.; Bykov, S. V.; Myshakina, N. S. *J. Phys. Chem. B* **2006**, *110*, 1928.
- (44) Mirkin, N. G.; Krimm, S. *J. Phys. Chem. A* **2002**, *106*, 3391.
- (45) Chan, H. Y. H.; Weaver, M. J. *Langmuir* **1999**, *15*, 3348.
- (46) Oklejas, V.; Sjostrom, C.; Harris, J. M. *J. Phys. Chem. B* **2003**, *107*, 7788.
- (47) Zou, S.; Weaver, M. J. *J. Phys. Chem.* **1996**, *100*, 4237.
- (48) Asher, S. A.; Mikhonin, A.; Bykov, S. *J. Am. Chem. Soc.* **2004**, *126*, 8433.
- (49) Torri, H.; Tatsumi, T.; Tasumi, M. *J. Raman Spectrosc.* **1998**, *29*, 537.
- (50) Herrebout, W. A.; Clou, K.; Desseyn, H. O. *J. Phys. Chem. A* **2001**, *105*, 4865.
- (51) Pimenov, K. V.; Bykov, S. V.; Mikhonin, A. V.; Asher, S. A. *J. Am. Chem. Soc.* **2005**, *127*, 2840.
- (52) Miura, T.; Hori-i, A.; Mototani, H.; Takeuchi, H. *Biochemistry* **1999**, *38*, 11560.
- (53) Barlow, S. M.; Hag, S.; Raval, R. *Langmuir* **2001**, *17*, 3292.
- (54) Trasatti, S. In *Advances in Electrochemistry and Electrochemical Engineering*; Gerischer, H., Tobias, Ch. W., Eds.; John Wiley: New York, 1977; Vol. 10, p 274.
- (55) Sokolowski, J.; Czajkowski, J. M.; Turowska, M. *Electrochim. Acta* **1990**, *35*, 1393.
- (56) Trasatti, S. Electrified Interfaces in Physics. In *Chemistry and Biology*; Guidelli, R., Ed.; Kluwer Academic Publishers: Dordrecht, The Netherlands, 1992; p 245.
- (57) Xu, M.-M.; Yuan, Y.-X.; Yao, J.-L.; Han, S.-Y.; Wang, M. *J. Raman Spectrosc.* **2010**, *42*, 324.
- (58) Blomberg, F.; Maurer, W.; Rueterjans, H. *J. Am. Chem. Soc.* **1977**, *99*, 8149.
- (59) Toyama, A.; Ono, K.; Hahimoto, S.; Takeuchi, H. *J. Phys. Chem. A* **2002**, *106*, 3403.
- (60) Kim, J. K.; Kim, Y.; Lee, S. Y.; Joo, S.-W. *Spectrochim. Acta A* **2008**, *69*, 286.
- (61) Martusevicius, S.; Niaura, G.; Talaikytė, Z.; Razumas, V. *Vibr. Spectrosc.* **1996**, *10*, 271.
- (62) Carter, D. A.; Pemberton, J. E. *Langmuir* **1992**, *8*, 1218.
- (63) Ashikawa, I.; Itoh, K. *Biopolymers* **1979**, *18*, 1859.
- (64) Miura, T.; Satoh, T.; Hor-i, A.; Takeuchi, H. *J. Raman Spectrosc.* **1998**, *29*, 41.
- (65) Ramfrez, F. J.; Tunon, I.; Collado, J. A.; Silla, E. *J. Am. Chem. Soc.* **2003**, *125*, 2328.
- (66) Lombardi, J. R.; Birke, R. L. *J. Phys. Chem. C* **2008**, *112*, 5605.